Dalton Transactions

ROYAL SOCIETY OF CHEMISTRY

PAPER

View Article Online
View Journal

Cite this: DOI: 10.1039/d6dt00402d

Molecular mechanisms behind the potential genotoxicity of metal oxide nanoparticles: nucleoside deglycosylation pathway

Fredric G. Svensson, Björn H. Greijer, Timothe Guerin, Tatiana Agback, Peter Agback and Vadim G. Kessler *

Polyoxometalates (POMs) represent well-defined molecular models for metal oxide nanoparticles and provide valuable insight into their interactions with biomolecules. Here, we investigate the interaction of Keggin-type phosphotungstic ($H_3PW_{12}O_{40}$) and silicotungstic ($H_4SiW_{12}O_{40}$) acids with RNA-derived nucleosides cytidine and guanosine, showing for the first time that these POMs can act as catalysts for the deglycosylation of nucleosides and provide a possible molecular mechanism that facilitates this process. These systems provide useful molecular-level models for metal oxide nanoparticle–biomolecule interactions and potential RNA deglycosylation pathways. Six crystalline complexes were obtained and structurally characterized by single-crystal X-ray diffraction, revealing extensive hydrogen bonding networks and pronounced interactions between nucleobases and the POM surfaces associated with charge transfer. In several cases, catalytic deglycosylation of nucleosides occurred during crystallization, yielding nucleobase–POM complexes and providing direct structural evidence of nucleoside cleavage. Complementary solution studies performed by ^{1}H NMR demonstrated rapid and selective catalytic deglycosylation of guanosine by silicotungstate under acidic near-boiling conditions, following apparent first-order kinetics (k = 0.399 min^{-1}), whereas cytidine reacted rather slowly, yielding only trace amounts of cytosine complexes. Phosphotungstate anions revealed analogous but slower reactivity. Control experiments showed no comparable catalytic activity for TiO_2 nanoparticle models (TiBALDH) under identical conditions. The results highlight pronounced differences in reactivity between purine and pyrimidine nucleosides and emphasize the role of charge-transfer and hydrogen-bonding interactions in POM-mediated catalysis. These findings provide molecular-level insight into metal oxide–biomolecule interactions and support the use of POMs as tunable models for understanding potential RNA degradation pathways induced by metal oxide nanoparticles.

Received 14th February 2026,
Accepted 24th April 2026

DOI: 10.1039/d6dt00402d

rsc.li/dalton

Introduction

Small metal oxide nanoparticles have attracted considerable attention owing to their interactions with biomolecules, particularly in the context of therapeutic and diagnostic ("theranostic") applications.[1] Polyoxometalates (POMs), in particular, have been intensively studied for their antibacterial, antiviral, and anticancer properties, exhibiting complementary or synergistic effects with conventional pharmaceuticals.[2–4]

POMs are small, discrete oligonuclear metal-oxo species commonly with a negative charge and a diameter from about 1 nm, making them suitable model systems for larger metal oxide nanoparticles. The chemistry of POMs is highly tailorable, making them very powerful tools for studying interactions with biomolecules on the molecular scale. In some cases, the POM–biomolecule complex can be crystallized, thereby giving direct information about molecular interactions.[5–7] In particular, a variety of POMs have been studied for applications as nanozymes for peptide bond hydrolysis.[8,9] Common minerals are also known to promote protein degradation.[10]

Recently, small anatase–TiO_2 nanoparticles were demonstrated to possess significant antiviral activity towards the enveloped transmissible gastroenteritis virus but not towards the non-enveloped encephalomyocarditis virus. Complexation between envelope phospholipids and TiO_2, with the subsequent disruption of the viral envelope, was proposed as the mechanism for this inhibitory effect.[11] POMs have been well known for several decades to inhibit a range of RNA viruses.[12]

There is an ongoing discussion concerning the cytotoxicity of TiO_2 NPs and their potential to cause DNA strand breakage.[13] TiO_2 has generally been considered safe for cosmetic

Department of Molecular Sciences, Swedish University of Agricultural Sciences, Uppsala, Sweden. E-mail: vadim.kessler@slu.se

and food applications, *e.g.*, as a UV adsorber in sunscreens and as a food additive. However, its safety has recently been questioned, with claims of various negative consequences upon extended or high-dose exposure.[14] Interaction with the cell membrane and receptors and cytotoxicity *via* the formation of oxygen radicals upon photoactivation appear to be the main hazards.[15] Lojk *et al.*[16] studied the uptake and effects of several nanoparticles (SiO_2, Ag, and TiO_2) on human neural cells. They concluded that even at low exposure (2–10 μg ml^{-1}), especially under prolonged exposure, these nanoparticles could negatively affect the cells. Some recent works have reported DNA damage caused by TiO_2 nanoparticles.[17–19] However, a study by Rajapakse and co-workers[20] concluded that an erroneously conducted single cell gel electrophoresis assay ("Comet assay") used to detect DNA damage can cause false positives, especially if not complemented by other biomarkers for DNA damage. Naya and co-workers[21] investigated the effect of intratracheal instillation of anatase TiO_2 in rats. While the exposure induced inflammation, no DNA damage was found. However, UV-illumination of TiO_2 is known to cause DNA damage and strand breaks by generation of reactive oxygen species.[22,23]

In the present study, we have investigated the interaction between a pyrimidine (cytidine)- and a purine (guanosine)-derived RNA nucleoside, and Keggin POMs represented by phosphotungstic acid and silicotungstic acid. The purpose was to use these POMs as model systems for the potential catalysis of the deglycosylation reaction (RNA breakage) that might be exhibited by metal oxide nanoparticles. The deglycosylation reaction (the removal of a sugar group from, usually, a biomolecule) occurs naturally for purines and pyrimidines, although at very slow rates, but can be greatly accelerated by enzymes or catalysts.[24,25] UV-illumination and hydrolytic oxidation can also cause deglycosylation with potential resulting RNA/DNA damage.[26,27] Deglycosylation is performed enzymatically by DNA glycosylases as part of the base excision repair mechanism to remove damaged nucleobases.[28] For RNA, the *N*-glycosidic bond can be cleaved by RNA *N*-glycosidases.[29]

The spherical metal oxo-anions of about 1 nm provide excellent models for metal oxide nanoparticles for studying interactions between biologically relevant molecules. Phosphotungstic acid and silicotungstic acid bearing different charges (−3 and −4, respectively) and displaying different polarities of metal–oxygen bonds were specifically chosen in view of their previously demonstrated ease of crystallization with various biomolecules. As a comparison, titanium(IV) "bis (ammonium lactate)dihydroxide" (TiBALDH) was used specifically as a model for TiO_2 nanoparticles, as TiBALDH exists in a coordination equilibrium with TiO_2 nanoparticles of about 3 nm in size.[30] In this work, we aimed to isolate POM–nucleobase complexes and evaluating the potential stability and transformation pathways. We present the first observation of the catalytic function of two POMs, silicotungstic acid and phosphotungstic acid, for the deglycosylation reaction of nucleobases (cytidine and guanosine) and propose a possible molecular interaction pathway that facilitates the process.

Materials and methods

Chemicals

Phosphotungstic acid (Thermo Scientific, p.a., CAS: 12501-23-4), silicotungstic acid (Sigma-Aldrich, p.a., CAS: 12027-43-9), hydrochloric acid (Supelco, 37%, CAS: 7647-01-0), cytidine (Sigma-Aldrich, 99%, CAS: 65-46-3), guanosine (Sigma-Aldrich, 98%, CAS: 118-00-3), dopamine hydrochloride (Aldrich, 98%, CAS: 62-31-7), and TiBALDH (Sigma-Aldrich, 50 wt%, CAS: 65104-06-5) were used. The general synthetic procedure is illustrated in Scheme 1.

Preparation of molecular models

Compound **1**, $[(HCytidine)_3PW_{12}O_{40}]$: 0.109 g (0.59 mmol) cytidine and 0.432 g (0.150 mmol, 3 mM) phosphotungstic acid were mixed in 50 mL of 0.1 M HCl. The mixture was precipitated (yellow), heated to 95 °C to dissolve, and then allowed to cool to room temperature slowly in a Dewar flask. The pH of the freshly prepared solution was 1.40.

Compound **2**, $[(HCytidine)HPW_{12}O_{40}{\cdot}H_3O]$: 0.144 g (50 μmol, 1.1 mM) phosphotungstic acid was dissolved in 10 mL of 0.1 M HCl, and 0.012 g (50 μmol) cytidine was dissolved in 35 mL of 0.1 M HCl. The phosphotungstate solution was added to the cytidine solution. No precipitation occurred, and the pH of the colorless freshly prepared solution was 1.41. The solution was allowed to evaporate over several weeks until crystals formed.

Compound **3**, $[(HCytosine)\ PW_{12}O_{40}{\cdot}2H_3O]$: It was identified as a fraction in **2** after several attempts of re-crystallization by dissolving in 0.1 M HCl on heating and subsequent slow cooling.

Compound **4**, $[(HGuanine)H_2PW_{12}O_{40}]$: 0.288 g phosphotungstic acid (100 μmol) and 0.08 g (28.2 μmol, 2 mM) guanosine were dissolved in 50 mL of 0.1 M HCl. The pH of the freshly prepared solution was 1.36. A yellow precipitate was formed, which was dissolved by heating to 95 °C. The solution turned orange as it cooled, and orange crystals formed at 85 °C. The solution was cooled to 70 °C over several hours and then allowed to cool to room temperature. This treatment

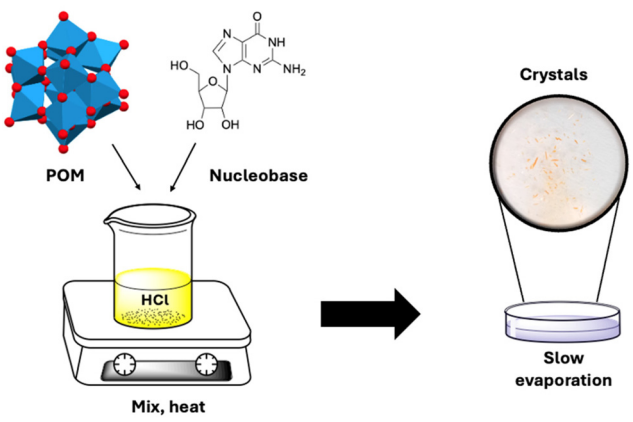

Scheme 1 General procedure for the preparation of compounds **1** to **6**.

appears to have removed the sugar group from guanosine, and only the guanine base is visible in the structure.

Compound **5**, [(Cytidine)$_6$(Dopamine)(SiW$_{12}$O$_{40}$)$_2$·9H$_2$O]: 100 mg of silicotungstic acid (34 μmol, 6.9 mM) was mixed with 1 eq. cytidine (8 mg, 34 μmol) and 0.5 eq. (7 mg, 17 μmol) dopamine in 5 mL of 0.1 M HCl. This colorless solution with a pH of 1.36 was left on a Petri dish for slow evaporation. Small, colorless needles were formed after about 2 weeks.

Compound **6**, [(Guanine)$_2$(SiW$_{12}$O$_{40}$)$_2$·16H$_2$O]: 100 mg of silicotungstic acid (34 μmol, 6.9 mM) in 5 mL of 0.1 M HCl was mixed with 1 eq. of guanosine (10 mg, 34 μmol). A yellow precipitate was formed, and the initial pH was 1.38. This solution was transferred into a glass tube and kept in a water bath at *ca.* 100 °C for 15 minutes and then cooled down to room temperature. After several months, small, pale yellow needle crystals were formed.

X-ray single crystal studies

All experiments were carried out at room temperature with a Bruker D8 Quest ECO diffractometer operating with MoKα-radiation (λ = 0.71073 Å). The details of data collection and refinement are summarized in Table 1 and in the SI. The initial solutions for all structures were obtained using direct methods, producing tungsten and heavy heteroelement, P or Si respectively, positions. All other non-hydrogen atom positions were identified in subsequent difference Fourier syntheses. The hydrogen atoms on the organic molecules were added through geometrical calculations where possible. No hydrogen atoms could be located on interstitial water molecules. The structure of Compound **1**, featuring **3** protonated cytosine cations per phosphotungstate anion, showed no disorder. The B-alerts in CheckCIF are caused solely by the impossibility to locate active hydrogen atoms on the sugar unit and interstitial oxygen atoms. Crystals of compound **2** were notoriously difficult to investigate due, on one hand, to rapid decomposition under X-ray beams at room temperature and cracking on cooling, preventing the possibility of using the cryo-system to obtain more complete data. This resulted in limited completeness of the data. This structure is an example of a hydrogen-bonded metal–organic framework with tunnel-shaped pores *ca.* 12 Å in diameter. The residual electron density in the pores is quite low, indicating that they are essentially empty in air-dried crystals. The crystals of compound **3** were discovered as minor impurity in the samples of **2** subjected to repeated re-crystallization by re-dissolution on reflux in water with subsequent slow cooling. This structure is free from disorder and does not contain additional oxygen atoms. There is only one symmetrically independent cytidine cation in a general position without disorder. The CheckCIF does not contain any A or B alerts. Compound **4** is chemically an analog of **3** with guanine instead of cytidine molecules. The structure is, however, heavily disordered, with one guanine molecule in the general position distributed equally between **3** partially overlapping locations. The other two are in a special position around a center of symmetry, overlapping with themselves,

Table 1 Crystallographic data of **1–6**. Additional crystallographic data are available in the SI Table S1 through S28

Compound	**1**	**2**	**3**	**4**	**5**	**6**
Composition	$C_{27}H_{42}N_9O_{55}PW_{12}$	$C_9H_{14}N_3O_{41.33}P_{0.83}W_{10}$	$C_{12}H_{18}N_9O_{43}PW_{12}$	$C_{15}H_{22}N_{15}O_5P_{12}$	$C_{53}H_{94}N_{16}O_{121}Si_2W_{24}$	$C_{10}H_{45}N_{10}O_{58}SiW_{12}$
Formula weight	3609.86	2689.87	3213.52	3369.65	7360.2	3467.85
Crystal system	Orthorhombic	Trigonal	Trigonal	Monoclinic	Triclinic	Monoclinic
Space group	$P2_12_12_1$	$P3$	$R\bar{3}$	$P2_1/n$	$P1$	$P21/n$
R_1	0.0379	0.0499	0.0239	0.0781	0.087	0.0396
w$R2$	0.0901	0.1362	0.0643	0.2269	0.1061	0.1105
GooF	1.148	1.034	1.054	1.035	1.009	1.107
a (Å)	13.5434(9)	25.309(3)	19.0192(9)	12.658(4)	13.097(5)	12.9065(17)
b (Å)	15.7745(11)	25.309(3)	19.0192(9)	18.893(6)	13.156(5)	24.994(3)
c (Å)	29.268(2)	15.307(2)	0.9800(14)	23.363(7)	23.538(9)	17.585(2)
α (°)	90	90	90	90	94.428(15)	90
β (°)	90	90	90	105.494(6)	90.250(15)	95.890(6)
γ (°)	90	120	120	90	112.309(14)	90
V (Å^3)	6252.9(7)	8491(2)	6572.3(2)	5384(3)	3738(3)	5642.8(13)
T (K)	295(2)	296(2)	295(2)	295(2)	293(2)	295(2)
Z	4	6	6	4	1	4
Nr. refl.	9952	9561	9343	9247	8512	9329
θ_{min}	2.42	2.28	2.66	2.34	2.46	2.47
θ_{max}	32.82	25.38	39.44	26.73	33.40	37.73
CCDC reference	2530303	2530304	2530306	2530305	2530307	2530308

which excludes the possibility of locating hydrogen atoms and causes the reported B-alerts in CheckCIF. Compound **5** is a rare case of a highly asymmetric polar structure with *P*1 as the space group. Crystallization of silicotungstate complexes can be rather difficult, in view of the high charge of the anion easily resulting in the formation of a glassy solid. Therefore, a small amount of more symmetric dopamine molecules has been added to change the steric conditions of packing. The resulting product contains 5 cytosine cations and one dopamine cation along with 4 phosphotungstate anions, resulting in 1.25 ligand-to-POM (or cation-to-anion) ratios, close to those in the structure of **2**. The structure of compound **5** is thus close to trigonal but severely distorted, resulting in *P*1 symmetry. Compound **6** is a clathrate structure with extremely high water content. Data collection was only possible on a crystal sealed into a capillary with a droplet of mother liquor on the bottom. Powder diffraction patterns were collected for compounds **2**, **4**, and **6** by placing crystals in glass capillaries. Theoretical powder diffractograms were calculated in CCDC Mercury version 2025–2.0.

The representative nature of the X-ray single crystal studies performed for the whole samples of produced crystals was additionally confirmed by recording at least **5** short diffraction experiments for each of the materials, randomly selecting crystals from the samples. Unit cell parameters were in each case coinciding with the standard deviations.

Full details of data collection and treatment in X-ray studies reported in this manuscript can be obtained by citing CCDC deposition numbers: 2530303–2530308.

Deglycosylation experiments

For the deglycosylation experiments, 100 mg (*ca.* 7 mmol) of phosphotungstate, silicotungstate, or the equivalent amount of titanium(IV) "bis(ammonium lactate)dihydroxide" (TiBALDH) was added to 5 mL of 0.1 M HCl with 1 equivalent of cytidine or guanosine in a glass test tube. The tubes were placed in a stirred water bath holding approximately 100 °C. Cytidine dissolved readily in 0.1 M HCl, but guanosine required heating to about 60 °C before dissolving. For the kinetic experiment, 0.5 mL aliquots of the solution were extracted at 1, 3, 5, 8, 12, and 20 minutes and transferred to Eppendorf tubes, which were snap-frozen in liquid nitrogen and stored in a freezer (−18 °C) until NMR analysis.

NMR analyses

The reaction solutions were analyzed with ^{1}H NMR, employing a Bruker Avance III 600 MHz spectrometer with Bruker TopSpin version 3.5. For sample preparation, 450 μL sample solution was mixed with 50 μL D_2O (Eurisotope) in a 3 mm NMR tube. For the reaction kinetics experiment, DMSO was used as the internal standard. The spectra were processed and analyzed using Bruker TopSpin version 4.0 software.

FTIR analysis

Transmission FTIR analyses of crystals and precipitates were carried out by grinding crystals or precipitates in dried KBr (200 °C, overnight) and pressing them to pellets (10 ton applied pressure for 3 minutes). A Perkin–Elmer FTIR spectrometer (Spectrum-100) was used to record the IR spectrum. Pure KBr was used for background subtraction. The spectra were recorded from 400 cm^{-1} to 4000 cm^{-1} with 1 cm^{-1} resolution and 16 scans per spectrum.

Results and discussion

Structural comments

Compound **1**, $[(HCytidine)_3PW_{12}O_{40}]$ (Fig. 1), crystallized in the orthorhombic space group *P*212121 as yellow plates. It contains 3 cytidine molecules per POM. The amino groups are

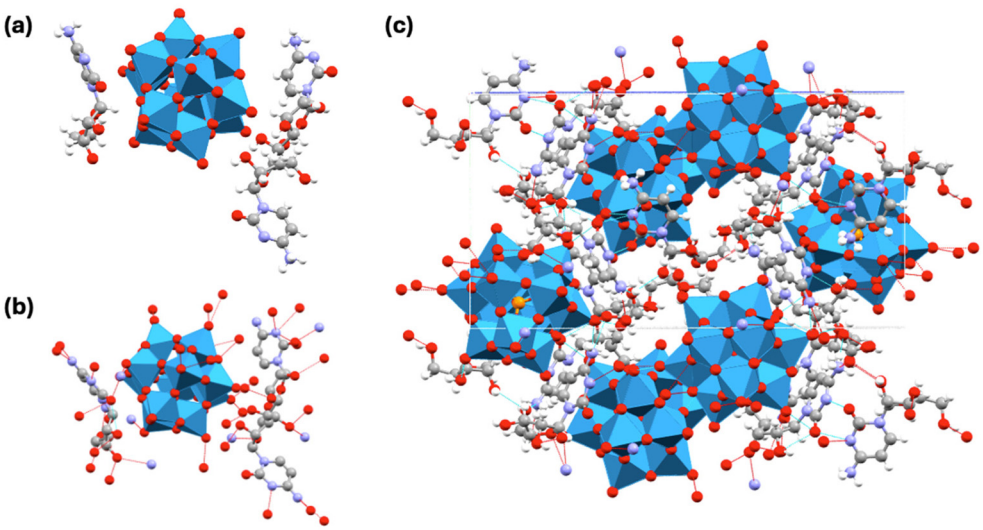

Fig. 1 Molecular structure of **1** $[(HCytidine)_3PW_{12}O_{40}]$ (a), hydrogen bonding in **1** (b), and packing with hydrogen bonding in **1** (c). Turquoise represents W, red represents O, orange represents P, grey represents C, blue represents N, and white represents H.

protonated to balance the −3 charge of the POM. However, the structure contains no solvent water molecules. The structure features an extended network of hydrogen bonds between the POM and cytidine, involving the nucleobase ammonium group and the ribose hydroxyl groups. Hydrogen bonding also occurs between cytidine molecules *via* ribose hydroxyls and nucleobase imine function. The shortest distances between the POM and nucleoside were in the following bonds: N3C–O31, 3.277 Å (terminal O), (C5C)H5CB–O32, 2.238 Å (bridging O) with the direct C209–O32 contact being 3.100 Å, and (O2C)H2CB–O19, 2.736 Å (terminal O) (SI Fig. S1).

Compound **2**, [(HCytidine)$HPW_{12}O_{40}\cdot H_3O$] (Fig. 2), crystallized in trigonal space group *P*3 as yellow needles. Like in structure **1**, cytidine has one protonated amino group, which with one oxonium ion balances the **2** negative charges of the POM. The packing features a hydrogen bonded framework between cytidine, POM and solvent water. The cytidine ammonium groups hydrogen bond to bridging oxygen atoms in the POM. The solvating oxonium ion hydrogen bonds to the nucleobase imine group. The amino bases are tilted in a face-on mode towards the POM, revealing substantial π–metal interactions. The aromatic ring acts as a π-acceptor of negative charge from polarized W–O bonds on the POM. From the extended packing in Fig. 2c, it can be seen that compound **2** forms an open MOF-like structure. The shortest distances between the POM and nucleoside were in the following bonds: N202–O35, 3.435 Å (terminal O), N202–O48, 3.469 Å (bridging O), (C209)H209–O21, 2.869 Å (bridging O) and (C208)H208–O21, 3.385 Å (bridging O) (SI Fig. S2).

Compound **3**, [(HCytosine)$H_2PW_{12}O_{40}$] (Fig. 3), crystallized in trigonal space group $R\bar{3}$ as yellow block crystals in trace amounts along with **2** after prolonged reflux in acidic medium. In this structure, the cytidine has been cleaved into cytosine, which crystallized in a 1 : 1 ratio with phosphotungstate. The ribose part was not present in the structure. The molecular packing is rather compact with alternating layers of phosphotungstate and cytosine. Also, for compound **3**, the cytosine aromatic ring is turned towards the POM, again forming a charge-transfer complex. Additionally, the amino group hydrogen bonds to both bridging and terminal oxygens on the POM. Hydrogen bonding also occurs between cytosine molecules, from the amino group to the carbonyl oxygen. The shortest distances between the POM and nucleoside were in the following bonds: (N1)H1B–O14, 2.783 Å (bridging O), (N3)H3A–O1, 2.645 Å (terminal O), and N2–O9, 3.454 Å (bridging O) (SI Fig. S3).

Compound **4**, [(HGuanine)$PW_{12}O_{40}\cdot 2H_3O$], crystallized in the monoclinic space group *P*21/*n* as orange needles (Fig. 4). The guanine molecule is heavily disordered over several positions. The −3 negative charge on the phosphotungstate is balanced by a protonated amine group on guanine and two oxonium ions. The guanine molecules are located face-on

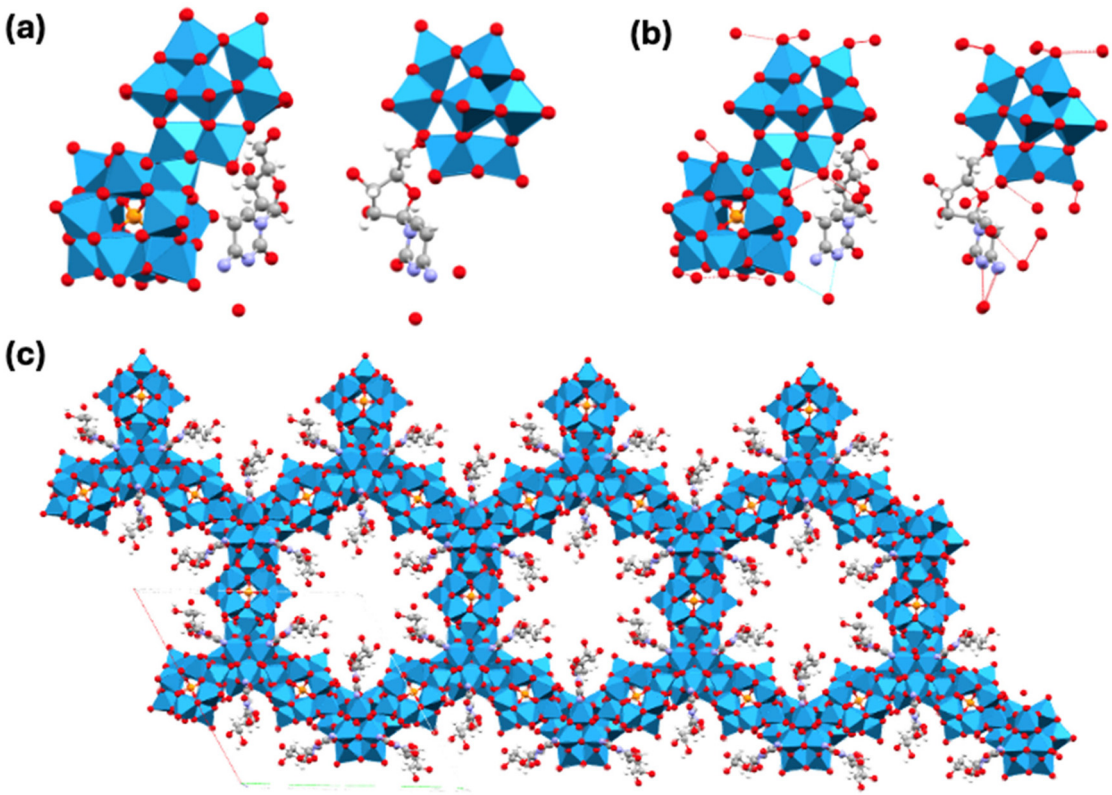

Fig. 2 (a) Molecular structure of **2**, [(HCytidine)$HPW_{12}O_{40}\cdot H_3O$], (b) hydrogen bonding in **2**, and (c) extended packing of **2** along the *b*-direction. Turquoise represents W, red represents O, orange represents P, grey represents C, blue represents N, and white represents H.

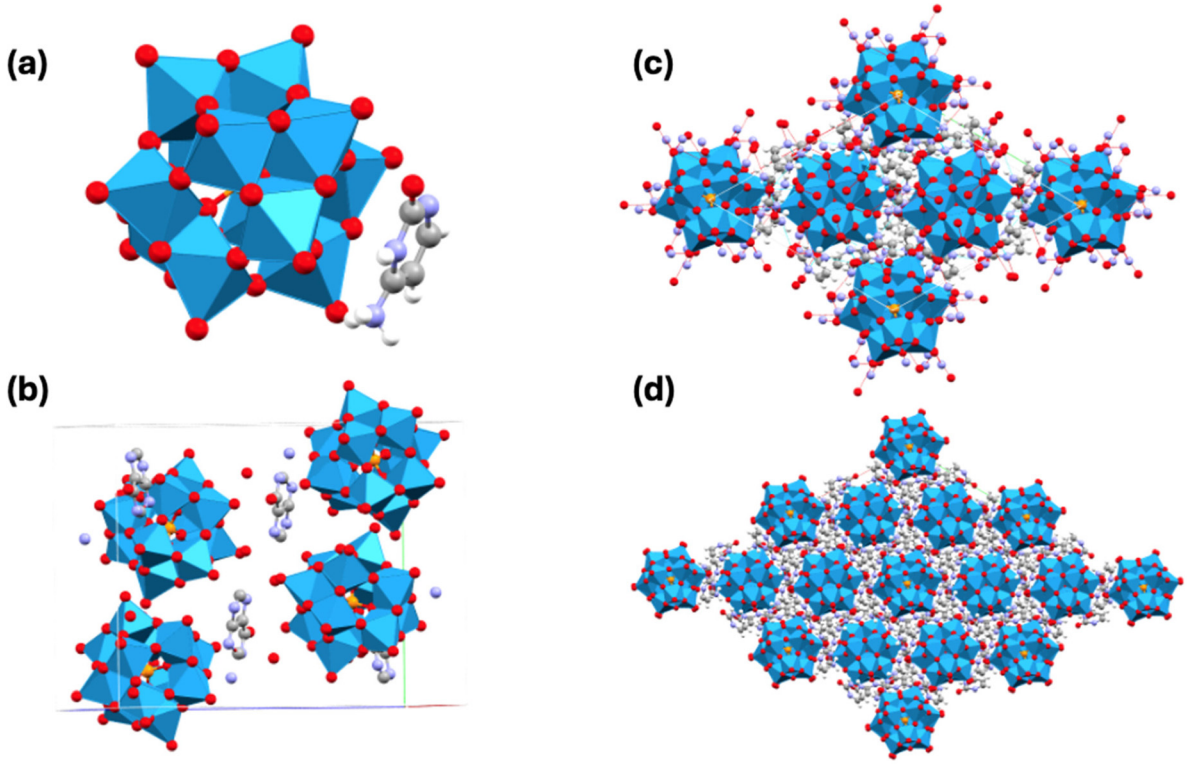

Fig. 3 (a) Molecular structure of **3**, [(HCytosine)$H_2PW_{12}O_{40}$], (b) packing of **2**, (c) packing of **2** with hydrogen bonds, and (d) extended packing of **3**. Turquoise is W, red is O, orange is P, grey is C, blue is N, and white is H.

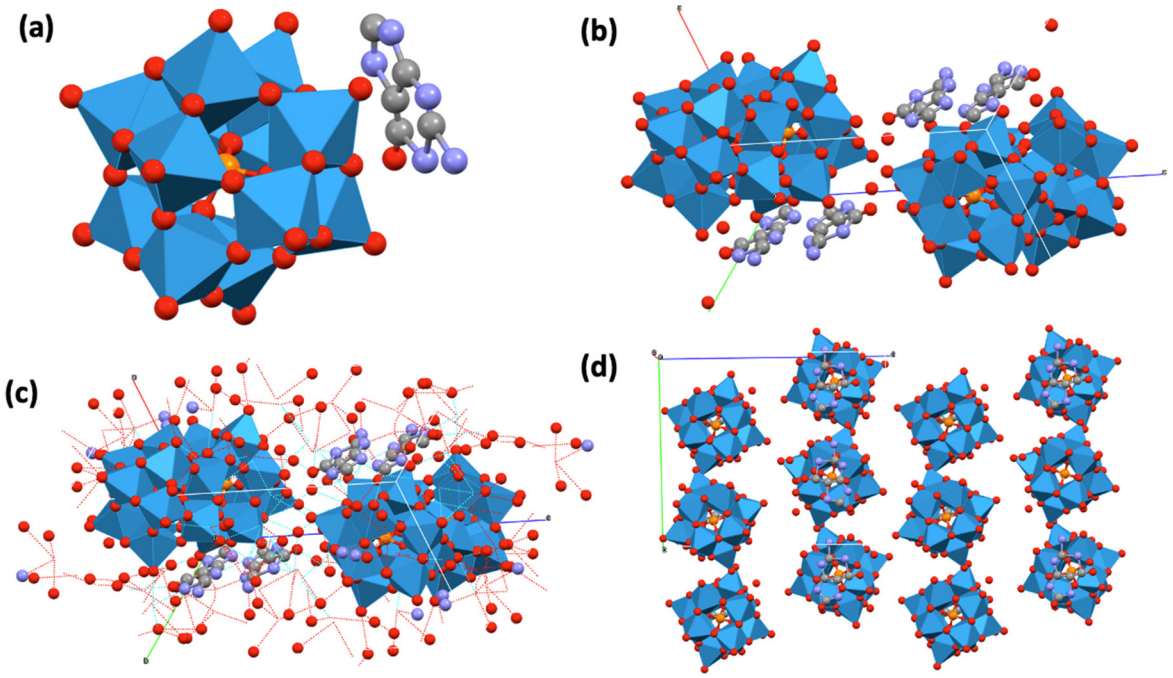

Fig. 4 (a) Molecular structure of **4**, [(HGuanine)$PW_{12}O_{40}{\cdot}2H_3O$], (b) packing of **4**, (c) hydrogen bonding in **4**, and (d) extended packing of **4** in the *c*-direction. Turquoise represents W, red represents O, orange represents P, grey represents C, and blue represents N. The heavy disorder in the guanosine molecule has been omitted for clarity.

towards the POM, which together with the orange color reveals charge-transfer interaction. However, the guanine amino group forms hydrogen bonds with the bridging oxygen atoms on the POM. The solvating oxonium ions form hydrogen bonds with the POM but not with the guanine. The extended structure forms alternating layers of POMs and guanine. The shortest distances between the POM and nucleoside were in the following bonds: N1A–O016, 3.555 Å (terminal O), N2A–O00, V 3.718 Å (bridging O), and N3A–O01F, 3.399 Å (SI Fig. S4).

Compound **5**, $[(HCytidine)_6(HDopamine)(SiW_{12}O_{40})_2{\cdot}9H_2O]$ (Fig. 5), crystallized in the triclinic space group *P*1 as colorless needles. Dopamine was added as 0.5 equivalents to phosphotungstate and cytidine in an attempt to facilitate formation of the 1 : 1 complex between phosphotungstate and cytidine. We previously utilized this strategy to prepare the 1 : 1 gamma-aminobutyric acid: phosphotungstate complex, which was unobtainable without the addition of dopamine (although dopamine itself was not incorporated into the crystal structure).[31] The cytidine nucleobases are turned face-on towards the POM, indicating π–donor-acceptor interactions. However, as the crystals are colorless, so the electronic transition appears to lie outside the visible region. Hydrogen bonding occurs between cytosine amino groups and bridging POM oxygen atoms. Hydrogen bonding also occurs between cytosine molecules *via* the amino groups and carbonyl oxygens. The shortest distances between the POM and nucleoside were in the following bonds: (CF5)H5FA–O15A, 2.904 Å (terminal O), N1F–O21A, 3.351 Å (bridging O), (C4F)H4F4–O21A, 3.302 Å (bridging O) (C4F)H4F4–O36A, 3.338 Å (terminal O), and N3F–H3F3–O22A, 2.715 Å (terminal O) (SI Fig. S5).

Compound **6**, $[(HGuanine)_2(SiW_{12}O_{40}){\cdot}14H_2O(H_3O)_2]$ (Fig. 6), crystallized in the monoclinic space group *P*21/*n* as small, pale-yellow needles. The unit cell contains 16 water molecules, and the crystals quickly degrade by water loss under ambient conditions. The experiment was carried out by sealing a crystal in an X-ray transparent borosilicate capillary, where a drop of mother liquor was placed in the bottom. Silicotungstate crystallized after several months, with guanine formed through the catalytic deglycosylation of guanosine at high temperature. Like in the previous structures, the nucleobase is turned face-on towards the POM. The yellow color indicates some charge-transfer. There is extensive hydrogen bonding in compound **6**. Guanine bonds *via* its amino group to bridging oxygens in the POM, to the carbonyl group of neighboring guanosines and to solvent water/oxonium ions *via* both the ammonium and carbonyl groups. The shortest distances between the POM and nucleoside were in the following bonds: N12–O38, 3.169 Å (terminal O), N12–O22, 3.252 Å (bridge O), N13–O2, 3.192 Å (terminal O), (N14)H14A–O2, 2.760 Å (terminal O), and (N11)H11C–O22, 3.127 Å (bridge O) (SI Fig. S6).

A general comment that should be given concerning the short contacts is that they mostly are due to hydrogen bonds between more acidic H-atoms of the protonated nucleobases and, primarily, more negatively charged bridging oxygen

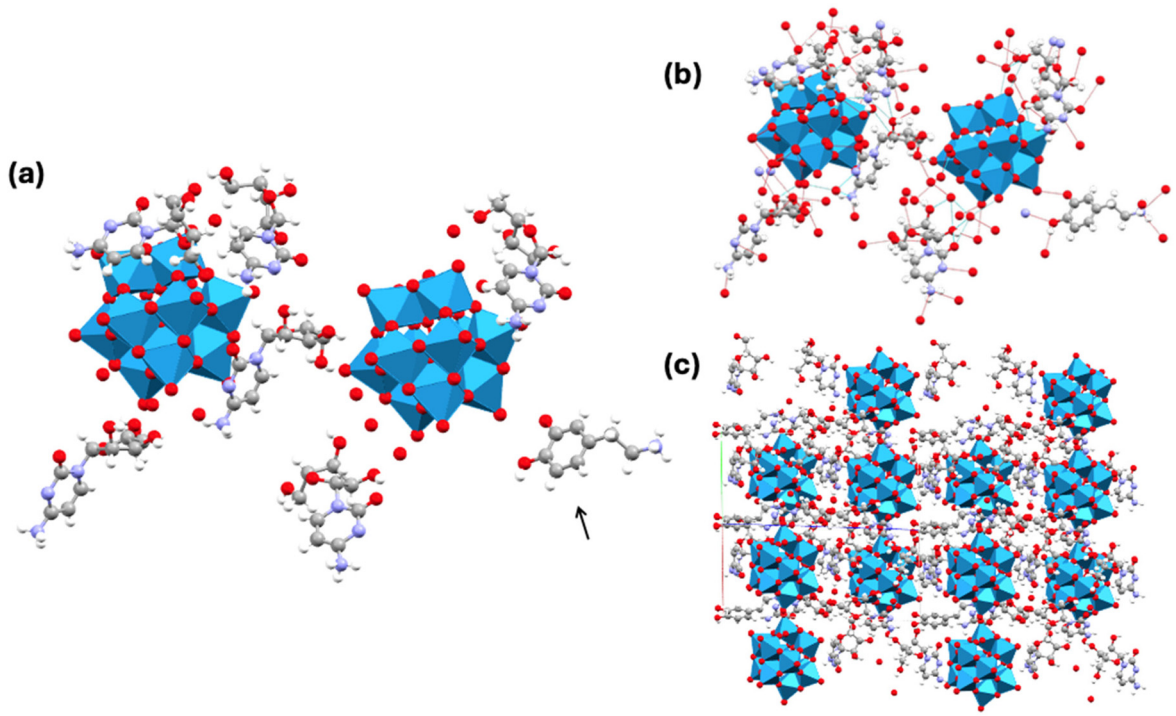

Fig. 5 (a) Molecular structure of **5**, $[(HCytidine)_6(HDopamine)(SiW_{12}O_{40})_2{\cdot}8H_2O(H_3O)]$, (b) packing of **5**, and (c) packing of **5** with hydrogen bonding. Turquoise represents W, red represents O, gold represents Si, grey represents C, blue represents N, and white represents H. The arrow indicates the lone dopamine group.

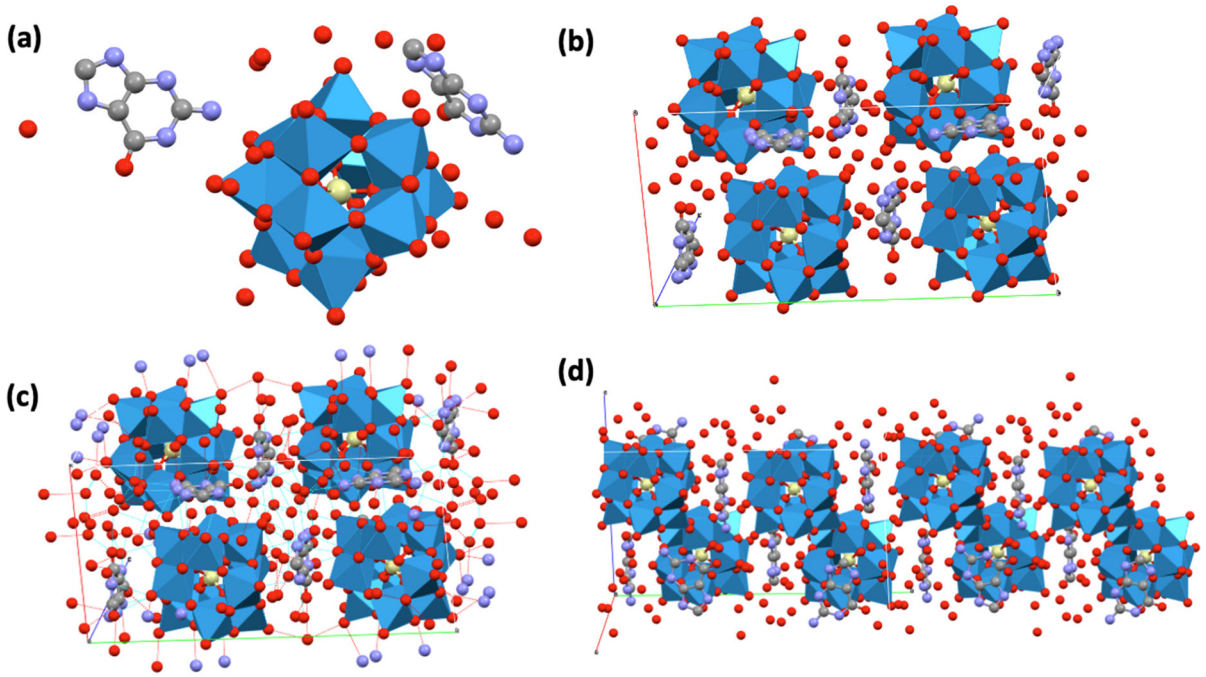

Fig. 6 (a) Molecular structure of **6**, $[(HGuanine)_2(SiW_{12}O_{40})\cdot 14H_2O(H_3O)_2]$, (b) packing of **6**, (c) packing of **6** with hydrogen bonding, and (d) extended packing in the *b*-direction. Turquoise represents W, red represents O, gold represents Si, grey represents C, blue represents N, and white represents H.

atoms of POMs, but sometimes even the terminal ones. An important additional phenomenon most apparent in the structure of compound **1** is a rather short distance between a bridging oxygen atom O32 in the structure of the POM and the carbon atom by which the sugar is connected to the nucleobase, C5C. This interaction indicates the role of POM as a nucleophile in the catalysis of the splitting of this C–N bond (Table 2).

FTIR analyses of complexes

Compounds **2**, **3**, **5** and **6** were obtained in large enough amounts for FTIR analysis (Fig. 7). A strong, quite broad band at *ca.* 800 cm^{-1} is assigned to W–O–W bending of the phosphotungstate ion. At 920 cm^{-1}, a sharp, strong signal is seen for terminal W═O. Another sharp band located at 1089 cm^{-1} is assigned to the P–O stretch; this is obviously absent in compound **5**, where the central phosphorous ion is replaced by Si. At about 1605 cm^{-1}, a small band from the C═C stretching of the aromatic rings is seen as well as a small band from the organic carbonyl groups at *ca.* 1720 cm^{-1}. A weak band for the C–N stretching is seen at 1270 cm^{-1}, originating from the purine and pyrimidine rings of the nucleobase and the amine group in dopamine. As the samples were dried prior to analysis, the water content is rather low.

Catalytic studies

The potential catalytic deglycosylation of guanosine and cytidine with two different POMs (silicotungstate and phosphotungstate) or TiBALDH was investigated (Fig. 8). The reaction was monitored by ^1H NMR by observing the decrease in the intensity of the proton resonance at *ca.* 6.1 ppm corresponding to H1′, which is covalently bonded to the C1′ carbon of the

Table 2 Selected short distances between POM oxygens and nucleobases. These are shown in SI Fig. S1 through S6

Compound **1**	Compound **2**	Compound **3**	Compound **5**	Compound **4**	Compound **6**
N3C–O31 3.277 Å	N202–O35 3.435 Å	(N1)H1B–O14 2.783 Å	(CF5)H5FA–O15A 2.904 Å	N1A–O016 3.555 Å	N12–O38 3.169 Å
(C5C)H5CB–O32 2.238 Å	N202–O48 3.469 Å	(N3)H3A–O1 2.645 Å	N1F–O21A 3.351 Å	N2A–O00V 3.718 Å	N12–O22 3.252 Å
(O2C)H2CB–O19 2.736 Å	(C209)H209–O2 1 2.869 Å	N2–O9 3.454 Å	(C4F)H4F4–O21A 3.302 Å	N3A–O01F 3.399 Å	N13–O2 3.192 Å
	(C208)H208–O21 3.385 Å		(C4F)H4F4–O36A 3.338 Å		(N14)H14A–O2 2.760 Å
			(N3F)H3F3–O22A 2.715 Å		(N11)H11C–O22 3.127 Å

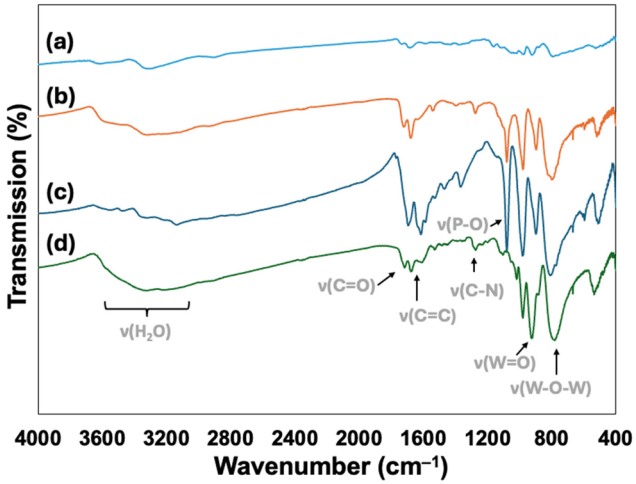

Fig. 7 FTIR spectra of (a) compound **6**, (b) compound **2**, (c) compound **3**, and (d) compound **5**. Major adsorption bands are indicated.

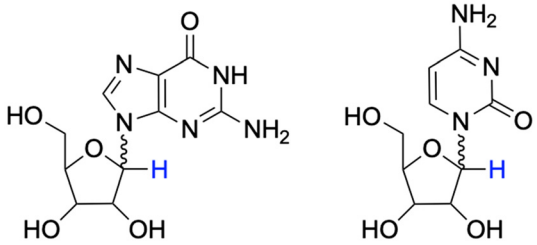

Scheme 2 Structures of (a) guanosine and (b) cytidine. The 1′ proton is highlighted in blue.

ribose ring (Scheme 2). Upon deglycosylation, this carbon replaces the nucleobase with an –OH group. Initially, the reaction was tested at 37 °C as this is relevant for biological systems. However, no reaction was observed at this temperature. When the reaction temperature increased to *ca.* 100 °C, guanosine was observed to undergo deglycosylation in the presence of silicotungstate (Fig. 8). Cytidine, on the other hand, remained intact even at this temperature. However, as revealed by the crystal structure of compound **3**, during prolonged treatment, cytidine together with phosphotungstate also underwent deglycosylation in acidic medium, although at a much slower rate than guanosine.

No change has been observed in the ^{1}H NMR spectrum of guanosine at 0.1 M HCl at 100 °C without silicotungstate, indi-

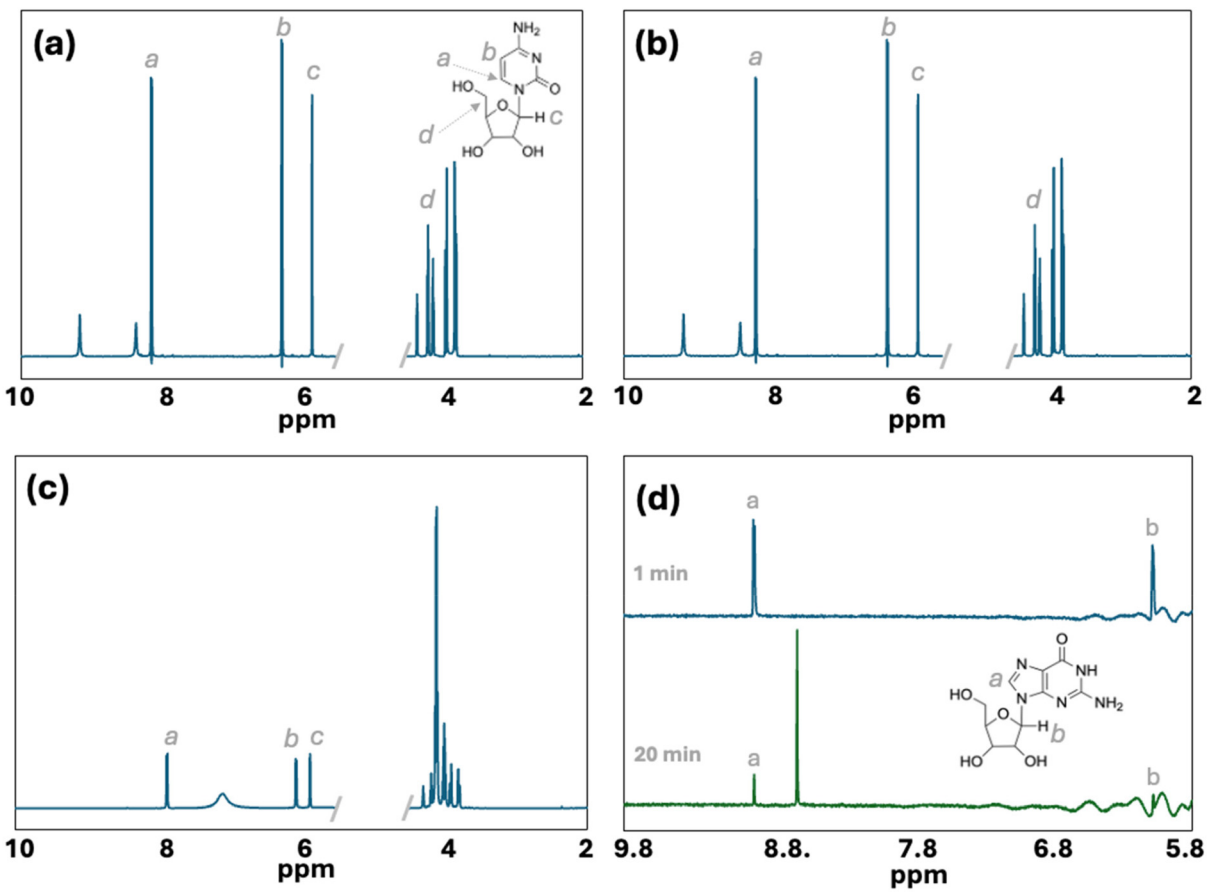

Fig. 8 ^{1}H NMR of (a) phosphotungstic acid with cytidine (1 : 1 at 100 °C), (b) silicotungstic acid with cytosine (1 : 1 at 100 °C), (c) TiBALDH with cytidine (1 : 1 at 100 °C), and (d) silicotungstic acid with guanosine (1 : 1) after 1 and 20 min at 100 °C. The water region from 4.5 ppm to 5.5 ppm was cut out in (a), (b), and (c) for clarity.

cating that it acts as a catalyst. Since silicotungstic acid is a strong acid and potentially could increase the acidity, pH was measured for guanosine in 0.1 M HCl and guanosine with SiW in 0.1 M HCl. In all cases, pH was 1.4 ± 0.2, suggesting that the reaction was not caused by a decreased pH but rather by a catalytic function induced by silicotungstate.

Guanosine is poorly soluble in water and requires dilute HCl as the solvent. Clear solutions were obtained first above 60 °C. Mixing 1 eq. of guanosine with TiBALDH diluted in deionized water led to the formation of a cloudy suspension, which cleared up upon heating. At 100 °C, the solution was clear, but as it was cooled down to room temperature, a white fluffy precipitate formed. This precipitate was washed (with deionized water), dried at 60 °C and analyzed by transmission FTIR (Fig. 9). Comparison of the precipitate with the reference guanosine revealed the precipitate to be pure guanosine. The ^{1}H NMR spectra of the supernatant showed only trace amounts of guanosine. Thus, under the present conditions, TiBALDH could not promote deglycosylation of either guanosine or cytidine. The oxygen atoms in the titania Ti–O bonds are expected to be more negative than those in (Si)W–O bonds. However, anatase TiO_2 has an isoelectric point of 5.9 to 6.2,[32] and the surface oxygens would therefore be protonated under acidic conditions. A catalytic activity at higher pH cannot be ruled out.

While cytidine remained stable, guanosine decomposed in the presence of silicotungstate under near-boiling conditions. To obtain a better understanding of the reaction, kinetic experiments were carried out. Small volumes were extracted from the reaction at different time points for 20 minutes. Since guanosine did not dissolve instantaneously, the first time point was set to 1 minute after adding it to the pre-heated silicotungstate solution. The kinetics were based on the decreasing 1′ hydrogen signal from the ^{1}H NMR spectra, using DMSO as the internal standard. As seen in Fig. 10a, the reaction is fast and is almost completed within 5 minutes. It approximately follows the first-order reaction kinetics (Fig. 10b). The rate constant was determined to be 0.399 min^{-1} from the slope of the first-order plot. The deglycosylation reaction of guanosine with silicotungstic acid is shown in Scheme 3. Kinetics analysis was performed on the mixture of phosphotungstic acid with guanosine using the same experimental conditions as those for silicotungstic acid and guanosine. It was, however, complicated due to the formation of

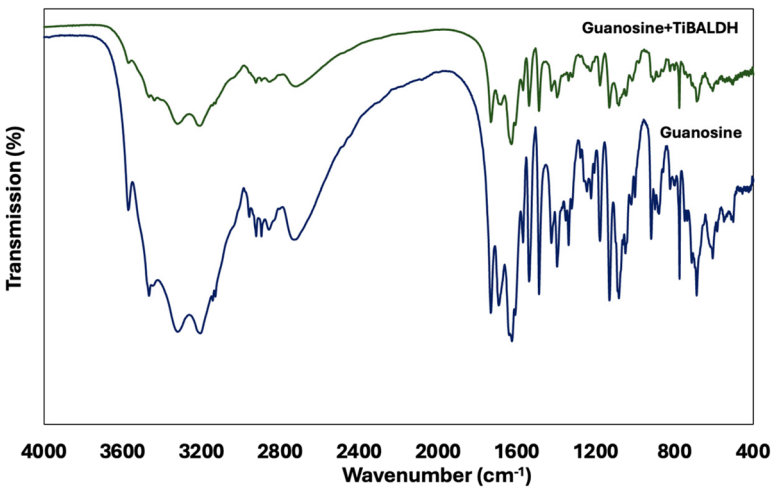

Fig. 9 Comparison of the FTIR spectra between reference guanosine and the precipitate after boiling guanosine with TiBALDH in basic medium.

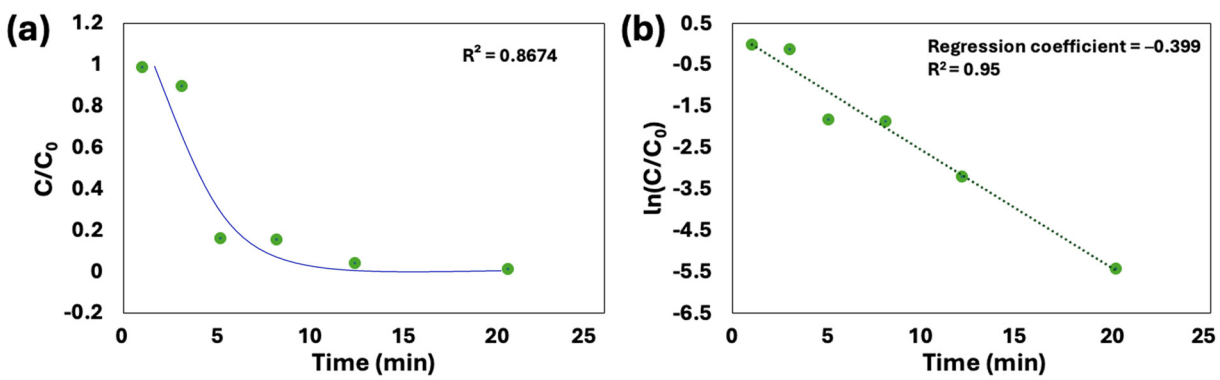

Fig. 10 Kinetic plots of the deglycosylation of guanosine by silicotungstate: (a) C/C_0 plot and (b) first-order plot.

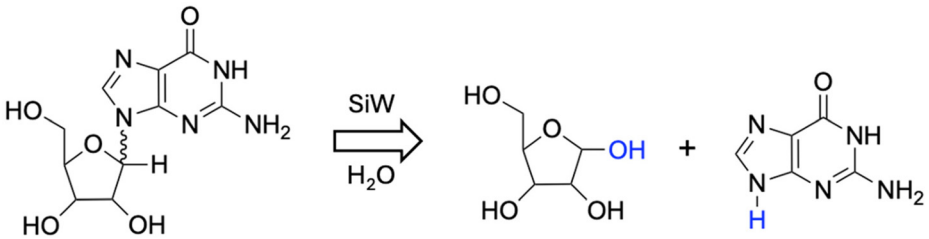

Scheme 3 Proposed degradation pathway of guanosine by silicotungstate.

massive precipitation when guanosine was mixed with silicotungstic acid. A clear solution was obtained first at about 100 °C, and it immediately re-precipitated in the pipette when taking out aliquots for the kinetics analysis, which complicated the analysis. The rate constant for the deglycosylation of guanosine by phosphotungstate was estimated to be 0.059 min^{-1} from the first-order plot (SI Fig. S9).

The combination of the obtained structural and kinetic data indicates that the actual mechanism in acidic deglycosylation of nucleosides is facilitated by a specific interaction of the POM with the C–N bond, where the negatively charged bridging oxygen atom in the POM acts as the nucleophile, facilitating charge separation and accumulation of positive charge on the affected carbon atom. The latter is then attacked by water as the replacing nucleophile, forming a hydroxyl group on the sugar molecule and protonating the released amino base. The observed difference between silico- and phosphotungstate appears thus logical in view of higher polarity in the POM core with less electronegative heteroelement atoms inside. This also explains the inactivity of titania nanoparticles in the proposed catalysis path, as in spite of possessing an even larger charge distribution in the Ti–O bond, they are protonated under the investigated reaction conditions. Negatively charged vanadium POMs have been observed to be contributing to the inhibition of Ca^{2+}–ATPase *via,* in the first hand, charge interactions between the POM and positively charged pockets of the enzyme.[33,34] The interaction we observed here differs principally from those between POMs and sugars, studied so far by NMR,[35] because the latter demonstrated only "normal" hydrogen bonds without any specific C···O(POM) interactions being detected. It is important to note that a key focus of further studies would be to address POM reactivity towards nucleotides bearing phosphate linkages. Vanadium-based POMs have, in fact, been observed to cleave phosphorylated organic species.[36] In this future work, we also expect a pronounced activity of titania particles in view of the high affinity of the TiO_2 surface to phosphate and phosphonate ligands demonstrated earlier.[37]

Diffusion-ordered NMR spectroscopy (DOSY) was attempted on 1 : 1 mixtures of silicotungstic acid or phosphotungstic acid with guanosine to study their interaction in solution. However, as the solubility of the mixtures was very low and as DOSY is much less sensitive than ^{1}H NMR, a reliable DOSY spectrum could not be obtained. A comparison between the ^{1}H NMR spectrum of guanosine in 0.1 M HCl and that of guanosine with 1 eq. silicotungstic acid in 0.1 M HCl is shown in SI Fig. S8. The two samples contain the same amount of guanosine, but as silicotungstic acid is added, the intensity sharply decreases.

Conclusions

In the current study, we have investigated the potential deglycosylation of RNA by metal oxide nanoparticles, using the polyoxometalates phosphotungstic acid and silicotungstic acid and nano-TiO_2 (TiBALDH) as model systems for the metal oxides. We chose guanosine as a purine nucleoside (RNA base "G") and cytidine as a pyrimidine nucleoside (RNA base "C"). We crystallized a number of structural models illustrating the interaction between the nucleosides and the polyoxometalates. It was found that phosphotungstate and silicotungstate were able to cleave cytidine and guanosine by deglycosylation. However, no deglycosylation was seen for nano-TiO_2 under the investigated conditions.

Kinetic studies revealed guanosine to be more rapidly degraded than cytidine. With silicotungstic acid as the catalyst, guanosine was almost completely degraded to its guanine and ribose components, while cytidine remained virtually intact. This suggests a difference in reactivity between the purine and pyrimidine nucleobases. Based on structural information from the molecular models, we see π–metal interactions where the aromatic ring acts as an acceptor of negative charge from the POM, forming charge-transfer complexes also supported by colored crystals. Both TiO_2 and the POM have negatively charged surfaces, though the POMs are much smaller than TiO_2.

Conflicts of interest

There are no conflicts to declare.

Data availability

Supplementary information (SI) is available including figures providing detailed insight into short contacts in the structures of compounds **3**, **4**, **5** and **6**, powder diffraction data for compounds **2**, **4** and **6**, NMR spectrum of free guanosine and its complex with silicotungstic acid, kinetics plots for guanosine deglucosilation catalyzed by phosphotunstic acid, and Tables with details of bonding in the structures **1**–**6**. See DOI: https://doi.org/10.1039/d6dt00402d.

CCDC 2530303–2530308 contain the supplementary crystallographic data for this paper.[38a–f]

All other experimental details (preparation and characterization details, including FTIR, NMR, *etc*.) are available on request from the authors.

Acknowledgements

Support from the Swedish Research Council (Vetenskapsrådet, project 2022-03971_VR, "Molecular mechanisms in oxide nanoparticle interactions with proteins") is gratefully acknowledged.

References

1 T. I. Shabatina, O. I. Vernaya, N. L. Shimanovskiy and M. Y. Melnikov, *Pharmaceutics*, 2023, **15**, 1181.
2 M. Aureliano, *Biochem.*, 2025, **2**, 8–26.
3 G. Guedes, S. Wang, A. H. Santos and F. L. Sousa, *Eur. J. Inorg. Chem.*, 2020, **22**, 2121–2132.
4 A. Bijelic, M. Aureliano and A. Rompel, *Angew. Chem., Int. Ed.*, 2018, **58**, 2980–2999.
5 B. H. Greijer and V. G. Kessler, *CrystEngComm*, 2025, **27**, 1679.
6 D. E. S. Marcano, N. D. Savic, K. Declerck, S. A. M. Abdelhameed and T. N. Parac-Vogt, *Chem. Soc. Rev.*, 2024, **53**, 84–136.
7 A. Nefedova, F. G. Svensson, A. S. Vanetsev, P. Agback, T. Agback, S. Gohil, L. Kloo, T. Tätte, A. Ivask, G. A. Seisenbaeva and V. G. Kessler, *Inorg. Chem.*, 2024, **63**, 8556–8566.
8 K. Declerck, N. D. Savic, M. A. Moussawi, C. Seno, R. Pokratah, J. D. Roo and T. N. Parac-Vogt, *J. Am. Chem. Soc.*, 2024, **146**, 11400–11410.
9 M. A. Moussawi, F. de Azambuja and T. N. Parac-Vogt, *Angew. Chem.*, 2025, **137**, e202423078.
10 S. S. Chacon, P. N. Reardon, C. J. Burgess, S. Purvine, R. K. Chu, T. R. Clauss, E. Walter, D. D. Myrold, N. Washton and M. Kleber, *Environ. Sci. Technol.*, 2019, **53**, 3018–3026.
11 B. Greijer, A. Nefedova, T. Agback, P. Agback, V. Kisand, K. Rausalu, A. Vanetsev, G. A. Seisenbaeva, A. Ivask and V. G. Kessler, *Nanoscale*, 2025, **17**, 3728–3738.
12 S. Shigeta, S. Mori, T. Yamase, N. Yamamoto and N. Yamamoto, *Biomed. Pharmacother.*, 2006, **60**, 211–219.
13 Y. F. Cao, J. Chen, Q. Bian, J. Ning, L. Yong, T. Ou, Y. Song and S. Wei, *Toxics*, 2023, **11**, 882.
14 S. Shabbir, M. F. Kuylar, Z. A. Bhutta, P. A. Boruah and M. Asif, *BioNanoScience*, 2021, **11**, 621–632.
15 Z. Lou, Z. Li, Z. Xie, I. M. Sokolova, L. Song, W. J. G. M. Peijnenburg, M. Hu and Y. Wang, *Small*, 2020, **16**, 2002019.
16 J. Lojk, J. Repas, P. Veranic, V. B. Bregar and M. Pavlin, *Toxicol. Res.*, 2020, **432**, 152364.
17 B. Trouiller, A. Westbrook and P. S. Schiestl, *Cancer Res.*, 2009, **69**, 8784–8789.
18 J. Petkovic, B. Zegura, M. Stevanovic, N. Drnovsek, D. Uskokovic, S. Novak and M. Filipic, *Nanotoxicology*, 2010, **5**, 341–353.
19 M. Carriere, M. E. Arnal and T. Douki, *Mutat. Res., Genet. Toxicol. Environ. Mutagen.*, 2020, **854**, 503198.
20 K. Rajapakse, D. Drobne, D. Kastelec and R. Marinsek-Logar, *Nanotoxicology*, 2012, **7**, 1043–1051.
21 M. Naya, N. Kobayashi, M. Ema, S. Kasamoto, M. Kukumoro, S. Takami, M. Nakajima, M. Hayashi and J. Nakanishi, *Regul. Toxicol. Pharmacol.*, 2012, **62**, 1–6.
22 J. Petkovic, T. Kuzma, K. Rade, S. Novak and M. Filipic, *J. Hazard. Mater.*, 2011, **196**, 145–152.
23 E. J. Petersen, V. Reipa, S. S. Watson, D. H. Stanley, S. A. Rabb and B. C. Nelson, *Chem. Res. Toxicol.*, 2014, **27**, 1877–1884.
24 K. S. Gates, *Chem. Res. Toxicol.*, 2009, **22**, 1747–1760.
25 R. B. Stockbridge, G. K. Schroder and R. Wolfenden, *Bioinorg. Chem.*, 2010, **38**, 224–228.
26 Y. Zhou, Z. Zhao, Q. Wu, J. Lei, H. Cui, J. Pan, R. Li and H. Lu, *Anal. Chem.*, 2024, **96**, 17576–17585.
27 T. Prashar, F. De La Selle and K. A. Hudak, *RNA Biol.*, 2023, **20**, 348–358.
28 A. L. Jacobs and P. Schär, *Chromosoma*, 2012, **121**, 1–20.
29 Y. Endo and K. Tsurugi, *J. Biol. Chem.*, 1988, **263**, 8735–8739.
30 G. A. Seisenbaeva, G. Daniel, J. M. Nedelec and V. G. Kessler, *Nanoscale*, 2013, **5**, 3330–3336.
31 F. G. Svensson, P. Simon and V. G. Kessler, *Inorg. Chim. Acta*, 2021, **526**, 120547.
32 M. Bischoff, N. Y. Kim, J. B. Joo and A. Marchioro, *J. Phys. Chem. Lett.*, 2022, **13**, 8677–8683.
33 B. R. Brito, H. d. S. Camilo, A. F. da Cruz, R. R. Ribeiro, E. L. de Sá, C. C. de Oliveira, G. Fraquez, G. Klassen, M. Aureliano and G. G. Nunes, *Inorganics*, 2025, **13**, 306.
34 I. Meskini, F. Capet, G. Fraqueza, N. Dege, M. N. Tahir, B. Ayed and M. Aureliano, *Molecules*, 2025, **30**, 4334.
35 C. F. G. C. Geraldes, M. M. C. A. Castro, M. E. Saraiva, M. Aureliano and B. A. Dias, *J. Coord. Chem.*, 1988, **17**, 205–219.
36 M. Aureliano, J. Leta, V. M. C. Madeira and L. de Meis, *Biochem. Biophys. Res. Commun.*, 1994, **201**, 155–159.
37 F. G. Svensson, G. Daniel, C. W. Tai, G. A. Seisenbaeva and V. G. Kessler, *RSC Adv.*, 2020, **10**, 6873–6883.
38 (*a*) CCDC 2530303: Experimental Crystal Structure Determination, 2026, DOI: 10.5517/ccdc.csd.cc2qxzpb; (*b*) CCDC 2530304: Experimental Crystal Structure Determination, 2026, DOI: 10.5517/ccdc.csd.cc2qxzqc; (*c*) CCDC 2530305: Experimental Crystal Structure Determination, 2026, DOI: 10.5517/ccdc.csd.cc2qxzrd; (*d*) CCDC 2530306: Experimental Crystal Structure Determination, 2026, DOI: 10.5517/ccdc.csd.cc2qxzsf; (*e*) CCDC 2530307: Experimental Crystal Structure Determination, 2026, DOI: 10.5517/ccdc.csd.cc2qxztg; (*f*) CCDC 2530308: Experimental Crystal Structure Determination, 2026, DOI: 10.5517/ccdc.csd.cc2qxzvh.